Electromagnetic Suitability Analysis and Characterization of Ultra-High Speed Spherical Steel Rotors

M. Schuck
T. Nussbaumer
J. W. Kolar

ETH
Eidgenössische Technische Hochschule Zürich
Swiss Federal Institute of Technology Zurich

Electromagnetic Suitability Analysis and Characterization of Ultra-High Speed Spherical Steel Rotors

Marcel Schuck[1], *Student Member, IEEE*, Thomas Nussbaumer[2] *Member, IEEE*, and Johann W. Kolar[1], *Fellow, IEEE*

[1]Power Electronic Systems Laboratory, Swiss Federal Institute of Technology, Zurich, Switzerland

[2]Levitronix GmbH, Zurich, Switzerland

The ongoing miniaturization trend of electric machines demands for higher rotational speeds to provide a required power level at decreased size. In this project, new concepts for bearingless machines with ultra-high rotational speeds exceeding 25 million rotations per minute (Mrpm) are researched. While the mechanical properties of the employed sub-millimeter size spherical steel rotors are documented, insufficient information is available on the electromagnetic characteristics which are crucial for magnetic levitation and acceleration. This study outlines the relations between the relative permeability and conductivity of the rotor material and the achievable active magnetic bearing force and angular acceleration. Measured results for complete hysteresis curves of different rotor steels are presented.

Index Terms—**ultra-high speed, magnetic bearing, asynchronous machine, spinning ball, material characterization.**

I. INTRODUCTION

INCREASING the rotational speed of an electric machine allows for achieving a required power level at decreased size, which has led to an ongoing miniaturization trend of machines with rising rotational speeds. The latter can be achieved by reducing bearing friction, which can effectively be facilitated by using magnetic bearings. Bearingless drive systems with rotational speeds of up to 1 Mrpm have been developed in the past [1]. By eliminating other losses that become significant at high rotational speeds, such as the air friction, much higher rotational speeds in excess of 20 Mrpm can be achieved. The highest reported rotational speed of 23.16 Mrpm was achieved with a steel sphere of 0.8 mm in diameter, which was magnetically levitated inside a vacuum tube and eventually destroyed due to the centrifugal load [2]. Since then, other reported attempts [3] did not succeed in achieving such high rotational speeds.

In this project new concepts for drives with ultra-high rotational speeds beyond 25 Mrpm are researched in order to extend the limits of conventional machines and overcome the challenges in regard to power density, mechanical stress and controllability of highly dynamic systems. The ultimate limit of the rotational speed is determined by the centrifugal load of the rotor. Therefore, small spherical rotors of diameters less than 1 mm made from ferromagnetic and conductive materials with high tensile strengths are used.

Small spheres made from various martensitic chrome steels and tungsten-carbide cobalt are used in ball bearings and are therefore readily available. The available characteristic data for these spheres is mostly limited to their mechanical properties in the aforementioned application, while insufficient information is available on the electromagnetic characteristics of the different materials. Yet, the latter are critical for assessing the achievable performance of the magnetic bearing and drive in the ultra-high speed motor application at hand. In this study, analytic models of the motor drive and magnetic bearing are provided and characteristic magnetic properties for different materials are obtained through measurements.

Section II briefly describes the motor setup and in Section III analytic models for the the achievable active magnetic
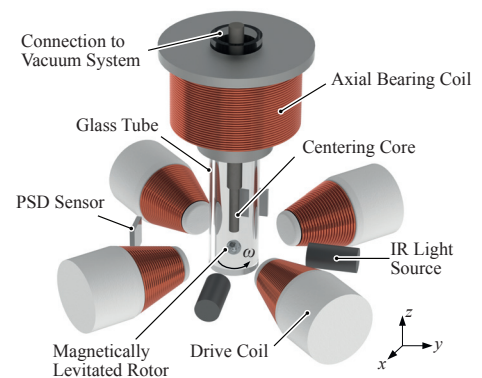
Fig. 1: Setup of the ultra-high speed motor.

bearing (AMB) force and motor torque dependent on the relative permeability and conductivity of the rotor material are derived. The aforementioned material properties were obtained experimentally through measuring complete hysteresis curves of different materials by directly using the spherical rotors as specimen in a vibrating sample magnetometer (VSM). The obtained results are presented in Section IV.

II. MOTOR SETUP

The developed ultra-high speed motor setup is shown in Fig. 1. The rotor is placed inside an evacuated glass tube to minimize air friction. Bearing friction is eliminated by using an axial magnetic bearing, which is constructed from a copper coil wound around a hollow ferromagnetic core to allow sufficient space for positioning of the vacuum tube through the core. A second, solid ferromagnetic cylinder is placed directly inside the vacuum tube to act as a centering core which concentrates the magnetic flux and is the center of attraction for the levitated rotor.

In addition to the axial bearing, four air coils are placed radially around the rotor to produce the fast rotational magnetic fields required for torque generation. Acceleration is achieved by the principle of a solid rotor induction machine, where eddy currents are induced inside the rotor, which are subject to tangential Lorentz forces.

As there is almost no air friction acting upon the rotor, radial oscillations due to disturbances are weakly damped, causing the magnetic suspension to become unstable. Therefore, the

radially-placed coils are also used as actuators for a radial AMB, which increases the radial damping of the system.

For the magnetic suspension to operate properly, the axial and radial rotor position has to be measured and controlled continuously. In the developed setup, the rotor is illuminated by two orthogonally-placed infrared light sources resulting in a rotor shadow being drawn onto two two-dimensional position sensitive device (PSD) sensors, which are placed on the opposite side of the vacuum glass tube. The resulting position signals are fed into digital PID controllers, which regulate the rotor position by adjusting the currents in the axial and radial bearing coils.

With the developed setup, spherical rotors with diameters of 3 mm down to sub-millimeter sizes can be levitated and accelerated.

III. Influence of Material Properties on Bearing and Drive Performance

To assess the influence of the characteristic rotor material parameters on the achievable magnetic bearing and drive performance of the ultra-high speed motor, analytic models for the achievable AMB force and motor torque are derived below.

A. Magnetic Bearing

Introducing a body made from magnetizable material, which is not a permanent magnet, into the external magnetic field $\vec{H}_{\text{ext}}$ with magnetic induction $\vec{B}_{\text{ext}} = \mu_0 \vec{H}_{\text{ext}}$ as generated by the bearing coil results in a magnetization $\vec{M}$ of this body. The latter is dependent on the value of $\vec{H}_{\text{ext}}$ and the magnetic properties of the rotor material as characterized by its B-H curve and results in a force originating from the interaction with the external induction $\vec{B}_{\text{ext}}$. The influence of the magnetic properties of the rotor material on the achievable AMB force is studied by applying magnetostatic principles. For providing analytic expressions, two simplifying assumptions are introduced, which have been verified by 2D and 3D finite-element-method (FEM) magnetic simulations to not have a negative effect on the accuracy of the developed force model:

1) The magnetization $\vec{M}$ of the sphere is uniform and is caused by the magnitude of the external magnetic induction $|\vec{B}_{\text{ext}}|$ at its center ($z = z_0$).
2) The magnitude of the external magnetic induction varies linearly over the diameter of the sphere, with its gradient being determined by $\frac{\partial |\vec{B}_{\text{ext}}(z_0)|}{\partial z}$.

In order to determine the bearing force, the magnetization and magnetic induction inside the sphere as caused by the external magnetic induction have to be determined first. For a sphere with uniform magnetization of magnitude M_0 as shown in Fig. 2 without an external magnetic field, the magnetic scalar potential in spherical coordinates can be found as (cf. [4])

$$\Phi_{M,\text{in}} = \frac{1}{3} M_0 r \cos(\theta) \qquad \Phi_{M,\text{out}} = \frac{1}{3} M_0 a^3 \frac{1}{r^2} \cos(\theta), \quad (1)$$

where a denotes the radius of the sphere. Consequently, the magnetic field and magnetic induction inside the sphere are

$$\vec{H}_{\text{in}} = -\frac{1}{3}\vec{M} \qquad \vec{B}_{\text{in}} = \mu_0(\vec{H}_{\text{in}} + \vec{M}) = \frac{2\mu_0}{3}\vec{M}. \quad (2)$$
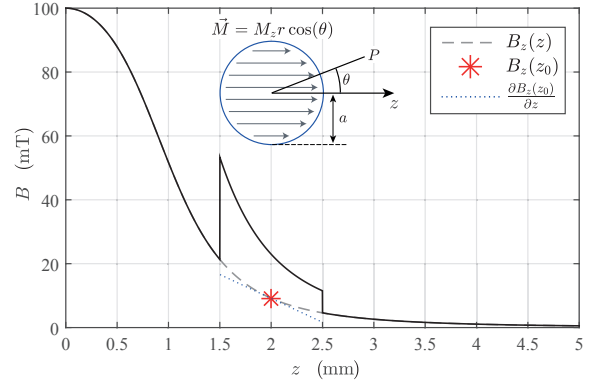

Fig. 2: Magnitude of the magnetic induction inside and outside of the sphere for varying distance from the AMB coil.

To obtain the field inside a magnetized sphere placed in an external magnetic induction $\vec{B}_{\text{ext}} = \mu_0 \vec{H}_{\text{ext}}$, the field components of (2) are superimposed with the external field, yielding

$$\vec{H}_{\text{in}} = \frac{1}{\mu_0}\vec{B}_{\text{ext}} - \frac{1}{3}\vec{M} \quad \vec{B}_{\text{in}} = \vec{B}_{\text{ext}} + \frac{2\mu_0}{3}\vec{M}. \quad (3)$$

From this, a general expression for the magnetic induction inside the sphere dependent on the external magnetic induction can be found by eliminating $\vec{M}$ as

$$\vec{B}_{\text{in}} + 2\mu_0 \vec{H}_{\text{in}} = 3\vec{B}_{\text{ext}}, \quad (4)$$

where the B-H curve of the rotor material relates $\vec{B}_{\text{in}}$ and $\vec{H}_{\text{in}}$ as $\vec{B}_{\text{in}} = \mu(|\vec{H}_{\text{in}}|)\vec{H}_{\text{in}}$ for isotropic materials. The resulting magnetic induction inside and outside the rotor are displayed in Fig. 2 for a sphere that has been introduced into the field of a cylindrical bearing coil, where z denotes the distance from the coil. The scaling of the field inside the rotor is clearly visible and the relevant variables for the subsequent force calculation are marked. In the absence of macroscopic conduction currents, the total magnetic force acting on a body with magnetization $\vec{M}$ and volume V which is bounded by a surface S can be obtained from the elementary force law as

$$\vec{F} = \int_V \rho_M \vec{B}_{\text{ext}} \mathrm{d}V + \int_S \sigma_M \vec{B}_{\text{ext}} \mathrm{d}S, \quad (5)$$

where $\vec{B}_{\text{ext}}$ denotes the applied magnetic induction, not including that of the body for which the force is being calculated. The concept has been employed that a magnetization $\vec{M}$ is equivalent to a volume current density $\vec{J}_M = (\vec{\nabla} \times \vec{M})$ and a surface current density $\vec{K}_M = (\vec{M} \times \vec{n})$. The magnetic volume charge density and magnetic surface charge density, which are used as mathematical equivalents to electric charges, are denoted by $\rho_M = -\vec{\nabla} \cdot \vec{M}$ and $\sigma_M = \vec{M} \cdot \vec{n}$, respectively. Assuming a uniform magnetization inside the sphere yields $\rho_M = 0$, and the first term in (5) becomes zero. Based on the uniform magnetization the magnetic surface charge is obtained as $\sigma_M = M_z \cos(\theta)$. Including the assumptions stated above, the external magnetic induction can be parametrized in spherical coordinates as

$$\vec{B}_{\text{ext}} = \begin{pmatrix} B_r r \sin(\theta) \\ 0 \\ B_z(z_0) + \frac{\partial B_z(z_0)}{\partial z} r \cos(\theta) \end{pmatrix}, \quad (6)$$
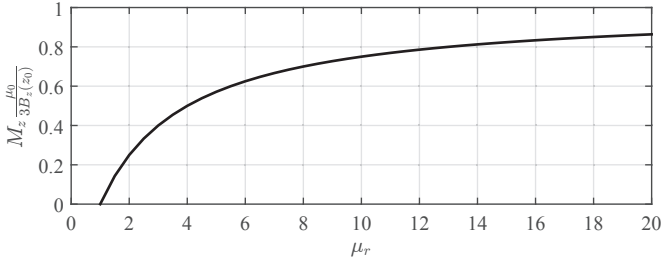
Fig. 3: Normalized magnetization of the sphere for different values of μ_r.

where B_r and $B_z(z_0)$ denote the radial component and the axial component at the center position of the sphere of the magnetic induction, respectively. By inserting (6) into (5), the resulting force is obtained as

$$\vec{F} = \frac{4}{3}\pi a^3 M_z \frac{\partial B_z(z_0)}{\partial z} \vec{e}_z. \tag{7}$$

As the magnetization of the sphere is directed into the same direction as the external magnetic induction, the resulting force is always directed towards the bearing coil, and its magnitude is dependent on the gradient of the external magnetic induction in z direction. It is independent of the radial component B_r, which can therefore be chosen arbitrarily in the parametrization of the field. The absolute value of the external field only affects the magnetization M_z of the sphere. If the relative magnetic permeability μ_r is assumed to be constant and hysteresis effects are neglected, (3) can be used to obtain an analytic expression for the magnetization as

$$M_z = \frac{3}{\mu_0}\left(\frac{\mu_r - 1}{\mu_r + 2}\right)B_z(z_0). \tag{8}$$

It is shown in Section IV that the aforementioned assumptions are well justified for suitable rotor materials. The presence of hysteresis is undesired in the considered AMB, as the resulting remanent magnetization in the absence of an external magnetic induction can cause undesired residual forces acting between the rotor and ferromagnetic parts of the AMB system. By inserting (8) into (7) it is apparent that, for given values of $B_z(z_0)$ and the gradient of the induction, the force increases rapidly for small increasing values of μ_r, while it levels off at high μ_r values. This behavior is illustrated in Fig. 3, where the normalized magnetization is plotted for different values of μ_r. Moreover, from the analytic expressions, it can be observed that the conductivity of the rotor material has no effect on the achievable magnetic force.

B. Torque Generation

A high torque is desirable to achieve fast acceleration of the rotor. The motor torque is generated by the interaction of the fast rotating magnetic field as generated by the drive coils and the induced eddy currents inside the rotor. A detailed analysis has been presented in [5], from which the influence of the rotor material properties on the drive performance can be studied. The general expression for the torque is derived as

$$\vec{T} = \underbrace{\frac{3\pi a^3}{1+\sqrt{2}}\frac{B_{\text{rot}}^2}{\mu_0}}_{T_{\text{bd}}}\underbrace{\frac{2+\sqrt{2}}{\sqrt{2}+q+\frac{1}{q}}}_{\xi}\vec{e}_z, \tag{9}$$

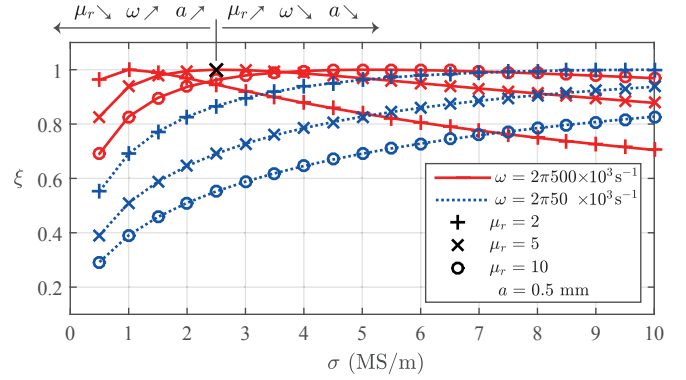

Fig. 4: Value of the breakdown torque scaling factor of (9) dependent on σ, μ_r, and ω.

TABLE I: Electromagnetic properties of different rotor materials

Material	σ / MS/m	μ_r (measured)
100Cr6	4.55	4.13
X105CrMo17	1.25	4.09
X45Cr13	1.81	4.14
X46Cr13	1.81	4.17
X47Cr14	1.38	2.85
TC3	-	3.46

where B_{rot} denotes the magnitude of the magnetic flux density used for torque generation, which is oriented in radial direction, and the sphere rotates around the z axis. The breakdown torque denoted by T_{bd} is the maximum achievable torque for a given rotor radius and magnetic flux density. The factor q in contains the variables corresponding to the material properties of the rotor material and is given as

$$q = \frac{1}{a}\sqrt{\frac{\mu_r}{\mu_0\sigma\omega}}, \tag{10}$$

where σ denotes the electrical conductivity of the rotor material and ω denotes the slip frequency, which is the difference between the frequency of the rotating magnetic field and the rotor spinning frequency. T_{bd} is obtained for $q = 1$ ($\xi = 1$) and the achievable torque is dependent on the combination of μ_r, σ, and ω, rather than on a single material property alone. It can be seen that the peak value of the scaling factor ξ is shifted based on the dependencies as illustrated in Fig. 4.

IV. ROTOR MATERIAL CHARACTERIZATION

To assess the suitability of different rotor materials for magnetic levitation and acceleration in the ultra-high speed motor based on the analytic relations provided in Section III, the relevant material properties were obtained through measurements. Spheres of small diameters are readily available, as they are commonly used in ball bearings. Table I lists common conductive materials with ferromagnetic behavior and their properties. While the conductivity of the material is usually given in the respective datasheet, insufficient information is available on the relative magnetic permeability. Therefore, the complete magnetization curves have been obtained through measurements, which were carried out using a VSM, cf. [6], [7], [8]. The advantage of this method is that the rotors can directly be used as specimen in an open circuit measurement, which allows to take material changes due to machining and
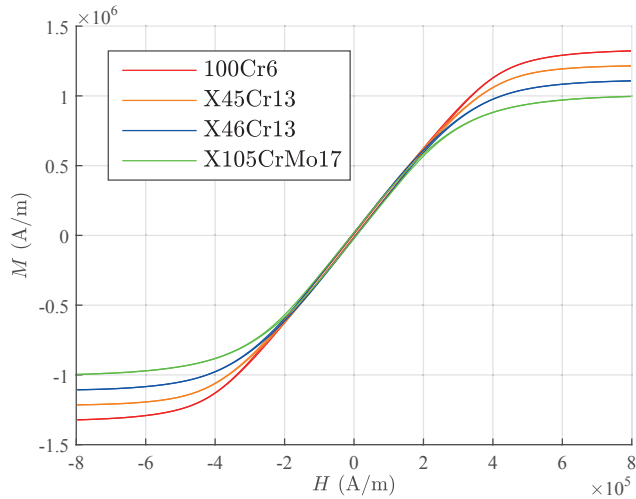
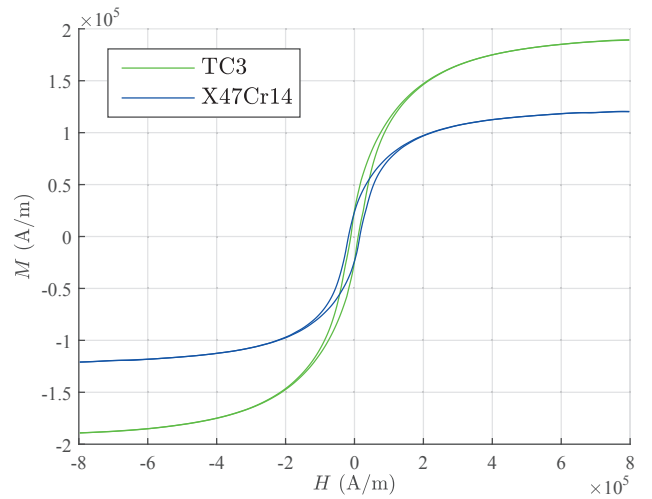Fig. 5: Measured magnetization curves of materials in group 1.

Fig. 6: Measured magnetization curves of materials in group 2.

thermal treatment [9] into consideration. Moreover, accurate measurement results can be obtained, as the instrument is calibrated with a spherical reference sample (e.g. chemically pure Ni $d = 1$ mm, cf. [10]), which allows to omit the compensation for the actual sample geometry affecting the measurement results [11], [12].

The rotor materials exhibit a largely isotropic behavior regarding their magnetic properties, which has been verified by repeated measurements after rotating the sample by $90°$. Due to the operating principle of the VSM, the magnetic moment $\vec{m}$ of the sample as a function of the applied magnetic field $\vec{H}$ is measured. If the specimen consists of an isotropic material, the magnetization M is easily obtained through dividing m by the volume of the sample. As the local μ_r of a material corresponds to the slope of the measured magnetization curve, it is calculated as

$$\mu_r = \frac{dM}{dH} + 1, \qquad (11)$$

where H is known from the measurements.

Figures 5 and 6 show the measured hysteresis curves for all listed materials of Tab. I, and the values of the initial relative permeability (μ_r at $H = 0$) have been added to the Table. It can be observed (Fig. 5) that the martensitic chrome steels denoted by the EN material numbers 100Cr6, X105CrMo17, X45Cr13, and X46Cr13 (group 1) exhibit very similar behavior regarding the initial values of μ_r with a narrow hysteresis loop as desired, and differ only in the magnetization at saturation. Contrarily, the materials referenced as X47Cr14 and TC3 (group 2) exhibit significantly different behaviors with lower initial μ_r, wider hysteresis and significantly lower values of the saturation magnetization (Fig. 6). While this behavior is explicable for the material TC3, containing high percentages of tungsten carbide and cobalt, by its high hardness, it is unexpected for X47Cr14, which is largely similar in its composition to the steels in the first group. Consequently, the steels in group 1 are equivalently well suited for magnetic levitation, while the materials from group 2 are less suitable as the achievable magnetic bearing forces are significantly lower, as outlined in the analyses above.

V. CONCLUSION

Analytic models for assessing the influence of the rotor material on the performance of the magnetic suspension system and the drive of an ultra-high speed motor have been provided. Together with the magnetization curves of various available materials, which have been obtained through measurements and were previously unavailable in the literature, suitable rotor materials were identified for usage in an ultra-high speed motor. The presented findings are universally applicable and exceed the previously available knowledge. They particularly allow the assessment of different steels in magnetic bearing applications.

ACKNOWLEDGMENT

REFERENCES

[1] C. Zwyssig, J. Kolar, and S. Round, "Megaspeed drive systems: Pushing beyond 1 million r/min," *IEEE/ASME Trans. Mechatronics*, vol. 14, no. 5, pp. 564–574, 2009.

[2] J. W. Beams, J. L. Young, and J. W. Moore, "The production of high centrifugal fields," *Journal of Applied Physics*, vol. 17, no. 11, pp. 886–890, 1946.

[3] A. Boletis and H. Bleuler, "Achieving ultra-high rotating speeds," in *8th International Symposium on Magnetic Bearing, Mito, Japan*, 2002, pp. 539–542.

[4] J. Jackson, *Classical electrodynamics*. New York: Wiley, 1999.

[5] T. Reichert, T. Nussbaumer, and J. W. Kolar, "Complete analytical solution of electromagnetic field problem of high-speed spinning ball," *Journal of Applied Physics*, vol. 112, no. 10, pp. –, 2012.

[6] S. Foner, "Versatile and sensitive vibrating-sample magnetometer," *Review of Scientific Instruments*, vol. 30, no. 7, pp. 548–557, 1959.

[7] S. Tumanski, *Handbook of Magnetic Measurements (Series in Sensors)*, 1st ed. CRC Press, 6 2011.

[8] F. Fiorillo, *Characterization and Measurement of Magnetic Materials*, 1st ed. Academic Press, 2 2005.

[9] D. Jiles, *Introduction to Magnetism and Magnetic Materials (International Business)*, 1st ed. Springer, 12 1990.

[10] R. Shull, R. McMichael, L. Swartzendruber, and S. Leigh, "Absolute magnetic moment measurements of nickel spheres," *Journal of Applied Physics*, vol. 87, no. 9, pp. 5992–5994, 2000.

[11] A. W. Pacyna and K. Ruebenbauer, "General theory of a vibrating magnetometer with extended coils," *Journal of Physics E: Scientific Instruments*, vol. 17, no. 2, p. 141, 1984.

[12] A. Zieba and S. Foner, "Detection coil, sensitivity function, and sample geometry effects for vibrating sample magnetometers," *Review of Scientific Instruments*, vol. 53, no. 9, pp. 1344–1354, 1982.